

## **CHAPTER 6**

### **Applications of high surface area porous nickel as a supercapacitor electrode material and as a hydrogen evolution catalyst**

In this chapter, we discuss the utility of the high surface area porous nickel obtained using template electrodeposition as a potential candidate for supercapacitor electrode material and as a hydrogen-evolving cathode in electrocatalysis. This chapter has been divided into two parts. The first part deals with the description of supercapacitors as electrochemical power source and the experiments carried out to characterize the porous nickel electrode as a supercapacitor material. In this case we do not limit our investigation to demonstration of a proof of a concept. Instead we show clearly the utility of the porous nickel material for device fabrication. The next part discusses the experiments performed to evaluate the high surface area nickel material as a potential candidate for a hydrogen-evolving cathode. We also compare our experimental results with the other existing nickel electrocatalysts and show that the high surface area porous nickel studied in this work performs as a good electrocatalyst.

#### **I. EVALUATION AS A SUPERCAPACITOR ELECTRODE MATERIAL**

##### **6.1. Introduction to supercapacitors**

The current research and development efforts on electrochemical power sources are mainly focused on fuel cells, batteries and electrochemical capacitors (EC) that are directed towards achieving high specific energy, high

specific power, long cycle life etc., at relatively low cost [1,2]. The electrochemical capacitors (EC) are often known by various names such as supercapacitors, ultracapacitors, power capacitors, gold capacitors, power cache, electrochemical double layer capacitors (EDLC) etc. and generally fall under the category of energy storage devices. Due to their high specific power, supercapacitors can find applications in high power devices such as lasers, automobile (for acceleration and for recuperation of brake energy) and space technologies [3,4]. A hybrid power source consisting of supercapacitor in parallel configuration to battery is proposed for applications in short duration pulse devices that require high specific power [5,6]. While a battery is a high energy and low power device, which is extensively used in conventional applications, the supercapacitor acts as a low energy and high power device and is ideal for use in high power pulse requirements [7]. Unlike a battery, supercapacitors possess a high power density with longer cycle-life time. They fill the gap between the batteries and conventional dielectric capacitors as can be observed in the Ragone plot [3,8], which is shown in figure 1. The Ragone plot is a plot of specific energy versus the specific power for various energy storage and energy conversion devices.

The supercapacitors also cover a wide range of specific energy density ranging from 0.05 Wh/kg to 15 Wh/kg and a specific power density from 10 W/kg to  $10^6$  W/kg [3]. There are two modes of energy storage mechanism operative in EC. One method is based on the double layer capacitance arising from the separation of charges at the electrode | electrolyte interface and the other one is based on the pseudocapacitance arising from the faradaic reactions occurring at or near the solid electrode surface due to the presence of electroactive materials. Generally, three different kinds of supercapacitors

based on carbon-carbon [9,10], transition metal oxides [11,12] and conducting polymers [13-15] have been reported in literature.

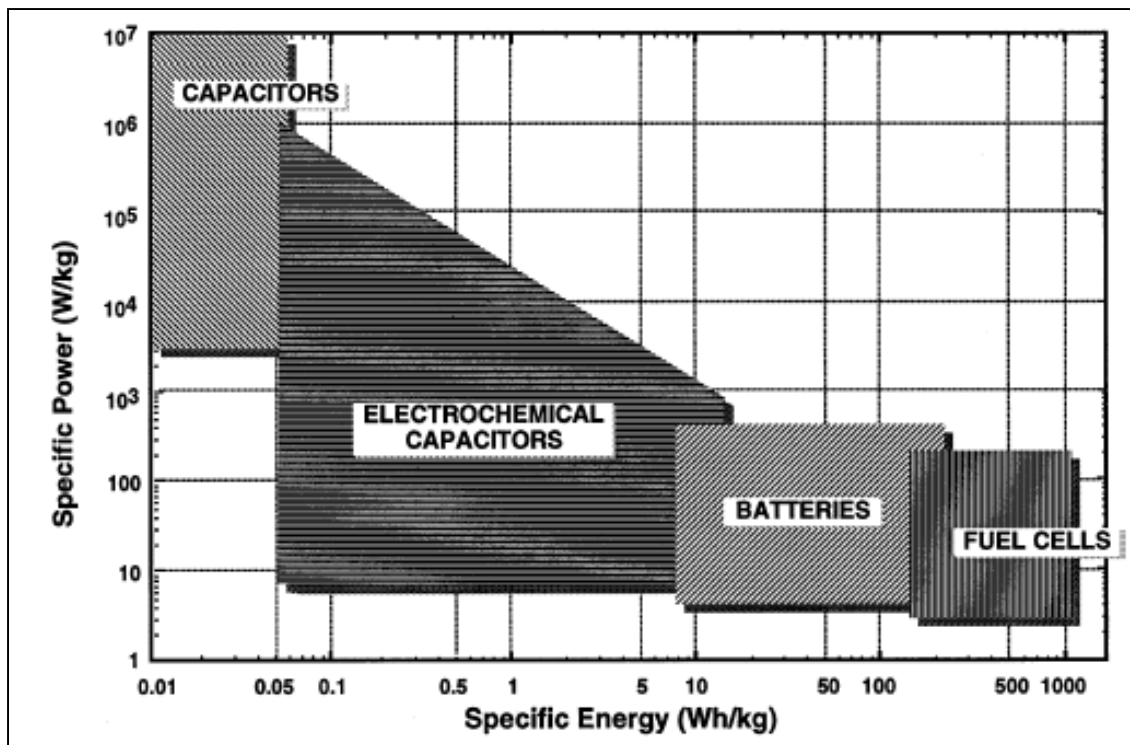


Figure 1: The Ragone plot for various energy storage and energy conversion devices.

The well-known electrochemical double layer capacitors (EDLC) are normally based on the usage of high surface area carbon materials such as activated carbon, carbon fiber cloth, carbon aerogels and foams as the electro active materials. A double layer capacitance of about 40  $\mu\text{F}/\text{cm}^2$ , which corresponds to a specific capacitance of 100-150 F/g was reported earlier [8,16]. The high specific capacitance values essentially arise from the high surface area of these materials. The utility of EDLC is limited by the maximum capacitance range (10-40  $\mu\text{F}/\text{cm}^2$ ), electrochemical stability of the electrolyte, the utilization of electrode surface area and the inherently associated high internal resistance [17]. Since the micropores of  $<2\text{nm}$  size, present in this case of supercapacitors that cannot be wetted by the electrolyte, a significant fraction

of the total area is inaccessible to the electrolyte, which limits its capacitance value [18]. To some extent, the problems associated with the wettability and accessibility can be improved by using conducting polymer as an electroactive material that depends mainly upon the size of the pores present within the polymer matrix [14]. In this case, the overall measured capacitance arises mainly from the pseudocapacitance contribution due to the redox reaction of conducting polymers [13-15]. The utility of supercapacitors based on the conducting polymers is limited by the stability of polymeric film and to a certain extent wettability and accessibility.

The other category of supercapacitor based on the transition metal oxides especially that of ruthenium oxide ( $\text{RuO}_2$ ) and Iridium oxide ( $\text{IrO}_2$ ) supercapacitors exhibit faradaic pseudocapacitance behaviour with huge specific capacitance values ranging from 720-760 F/g (for single electrode) [19]. Despite the impressive capacitance values and high reversibility obtained due to the faradaic redox reactions within these electroactive materials, the high cost of ruthenium and iridium has restricted its applications and the process of large-scale commercialization. There are several reports in literature on alternative electrode materials such as nickel oxide [17, 20-22], cobalt oxide [23] and manganese oxide [24], which are inexpensive and exhibit pseudocapacitive behaviour similar to that of ruthenium oxide being used as supercapacitors. Among them nickel oxide is attractive in view of its well-defined electrochemical redox activity and the possibility of enhanced performance through different preparative methods.

We find from the literature that there are several reports on nickel oxide as supercapacitor electrode material, which have specific capacitance values ranging from 240-277 F/g (for single electrode) [17, 20-22]. The preparation of NiO involves either sol-gel technique or electrochemical

deposition followed by heat treatment in air at around 300<sup>0</sup>C. There are studies on the effect of heat treatment, electrolyte environment and the potential range of operation on the measured capacitance values of nickel oxide electrodes. In addition to the higher specific capacitance values when compared to the carbon materials, the ability to produce thin films of NiO makes it an attractive material for high power devices. Park et al. reported an electrochemical capacitor based on a Ni(OH)<sub>2</sub>/activated carbon composite electrode with a specific capacitance value of 530 F/g (for single electrode) [25]. Nelson and Owen reported the fabrication of a supercapacitor/battery hybrid system based on the template deposited mesoporous Ni/Ni(OH)<sub>2</sub> positive electrode and a palladium negative electrode [26]. This system was able to deliver 166 mA h/g of Ni electrode in 50 ms at a mean discharge voltage of 1.18 V using 6M KOH aqueous solution. These values translate into an energy density of 706 kJ/kg and a power density of 14.1 MW/kg. Bursell et al. reported a hybrid supercapacitor based on ultrathin film of nickel [27] in which the Ni electrodes have been considered as the positive electrode in asymmetric supercapacitors. Since both the double layer capacitance and pseudocapitance are interfacial phenomena, the materials used for supercapacitors should possess a high specific surface area with good wettability of electrolyte to enhance their charge storage capability. As described in chapter 3, we have reported a method for the preparation of a high surface area porous nickel material by template electrodeposition using a hexagonal lyotropic liquid crystalline phase as a template [28], which was shown to be a potential candidate for supercapacitor electrode material recently [29]. The as prepared porous nickel material showed a roughness factor value of as high as 3620 indicating the formation of high surface area nickel making it a potential candidate for supercapacitor applications.

In this chapter, we describe the results obtained based on the experiments on some new symmetric and asymmetric supercapacitor cell assemblies based on the high surface area porous nickel and NiO electrodes with activated carbon as a negative electrode. The high surface area porous nickel material is obtained by template electrodeposition and the nickel oxide electrode is derived from the electrochemical oxidation of porous nickel [28]. We have used electrochemical techniques such as cyclic voltammetry (CV), electrochemical impedance spectroscopy (EIS) and charge-discharge transient analysis for the evaluation of porous nickel and NiO electrodes as supercapacitor electrode materials in an aqueous electrolyte of 6M KOH. The EIS data were analyzed in terms of complex power and complex capacitance values, from which the relaxation time constant ( $\tau_0$ ) and the figure of merit of supercapacitors have been determined. The charge-discharge profiles were used to calculate various parameters such as specific energy (SE), specific power (SP), specific capacitance (SC), columbic efficiency ( $\eta$ ) and equivalent series resistance (ESR) of the supercapacitors.

## 6.2. Experimental section

High surface area porous nickel material was prepared from a new hexagonal liquid crystalline phase consisting of 42 wt% Triton X-100, 5 wt% PAA and 53 wt% water in which the aqueous phase was replaced by nickel sulphamate bath [29], as described in chapter 3. After deposition, the roughness factor, which is a measure of true surface area of the porous nickel electrode, was determined using cyclic voltammetry by scanning the potential from  $-1.2$  V to  $-0.2$  V vs. SCE in 0.5M NaOH aqueous solution and measuring the charge under the anodic oxidation peak [28]. Activated carbon (Lancaster) having a

specific surface area of  $1500 \text{ m}^2/\text{g}$  was used as the negative electrode in asymmetric supercapacitor cell assemblies. The carbon paste was prepared using N-methylpyrrolidine as a binder and pasted onto a smooth nickel support that acts as a current collector. This carbon paste electrode was heated in an oven at around  $100^\circ\text{C}$  for about 15 minutes and then allowed to cool down to room temperature. Polypropylene membrane of thickness  $250\mu\text{m}$  was used as an electrode separator in the supercapacitor cell assemblies.

Electrochemical characterization of template deposited porous nickel electrode material in both the symmetric cell assembly (Porous Ni| KOH |Porous Ni) and the asymmetric cell assembly (Porous Ni| KOH |Activated carbon) of supercapacitors was carried out using cyclic voltammetry (CV), electrochemical impedance spectroscopy (EIS) and charge-discharge analysis. Cyclic voltammetry was performed in the double layer region of potential ranging from  $-1.1 \text{ V}$  to  $-0.9 \text{ V}$  in  $6\text{M KOH}$  aqueous solution at various potential scan rates. First, the high surface area porous Ni electrode was kept at a potential of  $-1.6 \text{ V}$  vs. SCE for 600s in the alkaline solution. This process reduces the surface oxides and cathodically cleans the surface by the evolution of hydrogen gas. This is followed by keeping the electrode at a potential of  $-1.02 \text{ V}$  vs. SCE, which oxidizes any metal hydrides on the surface [30]. Finally the supercapacitor cell was scanned in the double layer region to determine the capacitance.

Electrochemical oxidation of porous nickel to its corresponding nickel oxide had also been carried out to show that NiO obtained from the high surface area porous Ni can also be used as the supercapacitor electrode material. Porous Ni was converted into its corresponding NiO by potential scanning at the nickel oxide region [22,31]. First the potential was cycled between  $-0.1 \text{ V}$  and  $+0.5 \text{ V}$  vs. SCE in the alkaline solution for more than 25 cycles at various scan rates,

where the redox process of NiO formation and its stripping takes place. The capacitance was then determined by scanning the oxidized nickel oxide electrode in the potential range from  $-0.1$  V to  $+0.2$  V vs. SCE at different scan rates. The potential scan rates used for cyclic voltammetric experiments were varied from  $2$  mV/s to  $500$  mV/s. The capacitance was calculated by measuring the current separation ( $I$ ) from the cyclic voltammogram and the scan rate ( $v$ ) using the formula,  $C = I/v$ . In this case also both the symmetric as well as the asymmetric supercapacitor cell assemblies were analyzed.

Electrochemical impedance spectroscopic studies of supercapacitor cell assemblies were performed in  $6$ M KOH aqueous solution by applying a sinusoidal signal of  $10$ mV peak-to-peak amplitude at a frequency range of  $100$ mHz to  $100$ kHz. The impedance data were analyzed in terms of complex capacitance and complex power in order to determine the relaxation time constant ( $\tau_0$ ). The charge-discharge analysis was carried out at two different constant current densities of  $1$  mA/cm<sup>2</sup> and  $4$  mA/cm<sup>2</sup> at a potential range of  $0$  to  $1$ V for both the symmetric and asymmetric supercapacitor cell assemblies in  $6$ M KOH aqueous solution. All the electrochemical measurements were carried out using an EG&G Electrochemical Impedance Analyzer (model 6310) which can be operated both in dc and ac modes and interfaced to a personal computer (PC) through a GPIB card (National instruments). The charge-discharge analysis was performed in WonATech Automatic Battery Cycler, WBCS 3000 system interfaced to a computer. The analysis of data was carried out using WBCS V3.0 software and different parameters of the supercapacitor cell assemblies were calculated. All the chemical reagents used were AnalaR (AR) grade. Millipore water having a resistivity of  $18$  M $\Omega$  cm was used in all the experiments performed at room temperature.

## **6.3. Results and discussion**

### **6.3.1. Cyclic voltammetry**

#### **6.3.1.1. Using the high surface area porous nickel as an electroactive material**

Cyclic voltammetry is an important technique to evaluate the capacitive behaviour of any material. A perfect rectangular shaped voltammogram with a large current separation and symmetric in both cathodic and anodic directions are the indicators of an ideal capacitor. Figures 2 (a) and (b) show the cyclic voltammograms of symmetric (Porous Ni| KOH |Porous Ni) and asymmetric (Porous Ni| KOH |Activated carbon) supercapacitor cell assemblies in 6M KOH aqueous solution as the electrolyte. The potential scan rate was varied from 2 mV/s to 500 mV/s. It can be seen from the voltammograms that there is a large current separation between the forward and reverse scans with no visible peak formation, indicating a clear capacitive behaviour. It can also be observed that the voltammograms are not symmetrical about the zero current axis.

The fact that the voltammograms do not show perfect box type rectangular features with a mirror image characteristic implies that there is a substantial pseudocapacitance contribution to the overall measured capacitance. The capacitance values are determined by measuring the ratio of the magnitude of current separation and the scan rate. We have obtained a single electrode capacitance of  $1.4 \text{ F/cm}^2$  at 2 mV/s that corresponds to a specific capacitance value of 473 F/g.

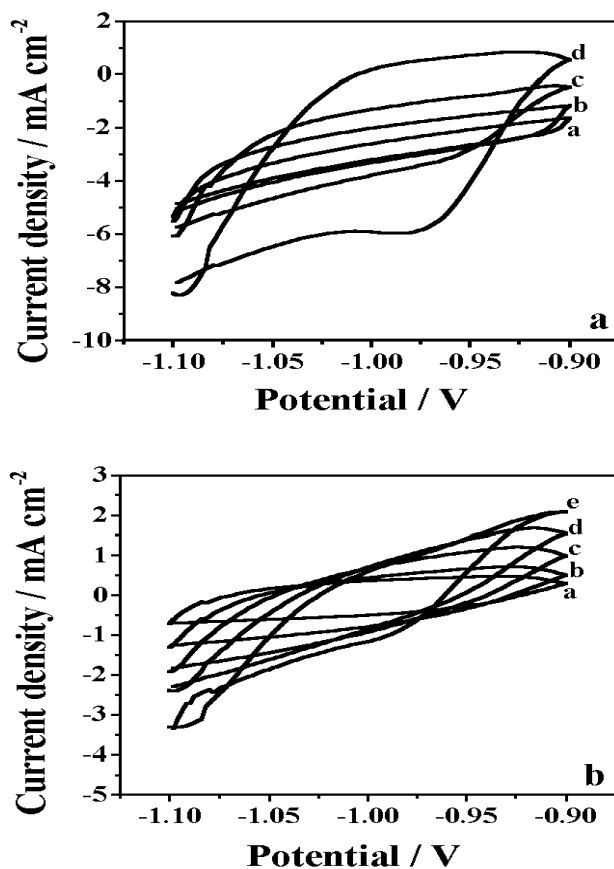


Figure 2: Cyclic voltammograms obtained using porous Ni cell assemblies of (a) Symmetric supercapacitor (Porous Ni| KOH |Porous Ni) at various scan rates of a) 50, b) 100, c) 200 and d) 500 mV/s and (b) Asymmetric supercapacitor (Porous Ni| KOH |Activated carbon) at various scan rates such as a) 25, b) 50, c) 100, d) 200 and e) 500 mV/s in 6M KOH aqueous solution.

The fact that all the CVs show almost rectangular features at 500 mV/s scan rate with high current density values indicates a good electrochemical activity and high power density. The unsymmetrical nature of the CVs arises due to a large reduction current owing to nickel hydride (NiH) formation, which is not completely oxidized during the forward cycle. Table 1 shows the double layer capacitance and specific capacitance values of the respective symmetric and asymmetric supercapacitor cell assemblies based on the high surface area porous nickel at different potential scan rates. It can be noted that the capacitance values vary with the scan rate. A maximum capacitance value of 66 mF/cm<sup>2</sup> is obtained at 100 mV/s scan rate for the symmetric supercapacitor, which corresponds to a specific capacitance of 22 F/g. A double layer capacitance of 250 mF/cm<sup>2</sup> corresponding to a specific capacitance of 84 F/g is obtained for the asymmetric supercapacitor at 2 mV/s. These values are quite low compared to a single electrode value of 473 F/g. It is speculated that the high ionic resistance inside the pores leads to a decrease in specific capacitance of the electrode material used in the symmetric cell assembly. The dependence of the measured specific capacitance on the scan rate is due to the contribution from pseudocapacitance arising out of the formation and subsequent oxidation of metal hydrides at this potential range [29].

**Table-1**

The double layer capacitance and specific capacitance values of symmetric and asymmetric supercapacitor cell assemblies based on the high surface area porous Ni electrode.

Scan rate (mV/s)	Double layer capacitance (mF/cm <sup>2</sup> )		Specific capacitance (F/g)	
	Ni  KOH  Ni	Ni  KOH  AC*	Ni  KOH  Ni	Ni  KOH  AC*
2	47	250	15.67	84.00
5	13	195	4.33	65.00
10	26	100	8.67	33.33
25	55	172	18.33	57.33
50	61	123	20.33	41.00
100	66	80	22.00	26.67
200	62	39	20.67	13.00
500	61	18	20.33	6.00

\* AC --- Activated carbon

### 6.3.1.2. Using the nickel oxide (NiO) electrode

Electrochemical oxidation method is employed to convert the high surface area porous nickel to its corresponding nickel oxide. In this case too both the symmetric (NiO| KOH |NiO) and asymmetric (NiO| KOH |Activated carbon) supercapacitor cell assemblies were investigated. Infact, the supercapacitors based on NiO show a better capacitive behaviour than the porous Ni electrode. Figures 3 (a) and (b) show the cyclic voltammograms of

symmetric and asymmetric supercapacitors based on NiO in 6M KOH aqueous solution respectively.

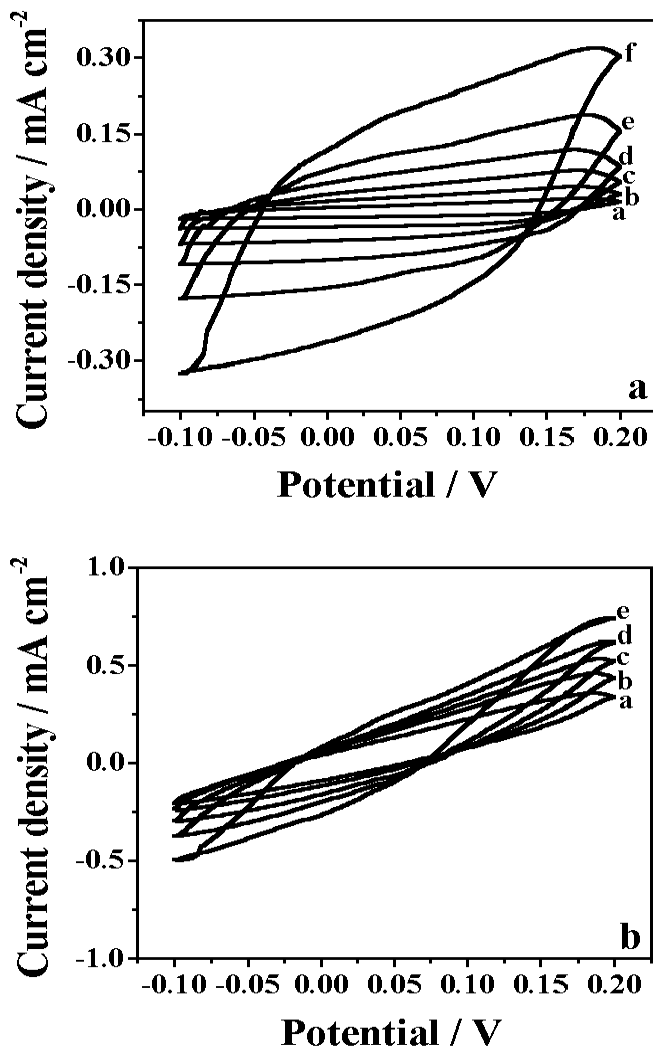


Figure 3: Cyclic voltammograms obtained using NiO cell assemblies of (a) Symmetric supercapacitor (NiO| KOH |NiO) at different scan rates such as a) 10, b) 25, c) 50, d) 100, e) 200 and f) 500 mV/s and (b) Asymmetric supercapacitor (NiO| KOH |Activated carbon) at different scan rates of a) 25, b) 50, c) 100, d) 200 and e) 500 mV/s in 6M KOH aqueous solution.

It is evident from the cyclic voltammograms that the supercapacitor cell assemblies show a large current separation with a mirror image characteristic especially at higher scan rates indicating a capacitive behaviour. There is no visible redox peaks formation. In this case also, the capacitance values are determined by measuring the ratio of the magnitude of current separation and the scan rate. A single electrode capacitance value of  $171 \text{ mF/cm}^2$ , which translates into a specific capacitance of  $57 \text{ F/g}$  has been determined at a scan rate of  $50 \text{ mV/s}$ . Table 2 shows the double layer capacitance and specific capacitance values of supercapacitors based on NiO, obtained at different potential scan rates. It can be seen that the capacitance values vary with the scan rate and the maximum capacitance value of  $15 \text{ mF/cm}^2$  is obtained at  $2 \text{ mV/s}$  for the symmetric supercapacitor, which corresponds to a specific capacitance value of  $5 \text{ F/g}$ . A double layer capacitance value of  $100 \text{ mF/cm}^2$  corresponding to a specific capacitance value of  $34 \text{ F/g}$  is obtained for the asymmetric supercapacitor at  $2 \text{ mV/s}$  scan rate. These values are of course quite less compared to a single electrode capacitance value of  $57 \text{ F/g}$  [29]. It can also be noted that the specific capacitance values are very much lower compared to the literature value of  $240$  to  $277 \text{ F/g}$  (for single electrode) and is due to the different procedures employed to obtain NiO in the present work. It is also felt that the lower values of capacitance obtained by the electrochemical oxidation method in our case may be due to incomplete conversion of nickel to its corresponding nickel oxide within the pores. We have restricted ourself to the double layer region for the capacitance measurement in order to avoid the contribution from pseudocapacitance arising out of the redox reaction. It can be concluded that the asymmetric cell assembly provides a higher capacitance value in both the cases of porous nickel and NiO electrodes, when compared to the symmetric cell assembly.

**Table-2**

The double layer capacitance and specific capacitance values of symmetric and asymmetric supercapacitor cell assemblies based on NiO obtained from the porous Ni electrode.

Scan rate (mV/s)	Double layer capacitance (mF/cm <sup>2</sup> )		Specific capacitance (F/g)	
	NiO  KOH  NiO	NiO  KOH  AC*	NiO  KOH  NiO	NiO  KOH  AC*
2	15	100	5.00	34.00
5	10	83	3.33	27.67
10	11	51	3.67	17.00
25	12	29	4.00	9.67
50	10	20	3.33	6.67
100	8	12	2.67	4.00
200	6	7	2.00	2.33
500	4	4	1.33	1.33

\* AC --- Activated carbon

To verify the pseudocapacitance contribution, we have studied the effect of scan rate on the capacitance of various symmetric and asymmetric supercapacitor cell assemblies based on the porous nickel and its corresponding nickel oxide electrodes. Figure 4 (a) shows the plot of I/v vs. scan rate (v) for the symmetric supercapacitor cell assembly of porous nickel and figure 4 (b) shows the variation of I/v vs. scan rate (v) for the other symmetric and asymmetric supercapacitor cell assemblies investigated in this work. The specific capacitance increases exponentially with decreasing scan rate for all the

supercapacitor cell assemblies except in the case of symmetric porous nickel cell assembly. Similar behaviour is reported in the literature for various electrode materials [32-35]. In the case of RuO<sub>2</sub> supercapacitor [34], this effect is attributed to increasing ionic resistance inside the pores leading to a decrease in its specific capacitance value. A similar effect is believed to occur in the present system where the surface reaction due to nickel hydride formation contributes to a large pseudocapacitance value. The incomplete formation and subsequent oxidation of nickel hydride at higher scan rates can lead to lowering of the measured capacitance with the increasing scan rate as can be observed in figure 4 (b). The formation of nickel hydride in alkaline media is well established in the literature [36-38]. The contribution of substantial pseudocapacitance to the overall measured capacitance is also suggested by the scan rate dependence of the specific capacitance. In the case of symmetric porous nickel supercapacitor, the capacitance increases with the scan rate. It is evident that the porous nickel electrode exhibits a good power characteristic, which can be inferred from the linear variation of current density with the scan rate observed in this case. We also felt that at higher scan rates, the pseudocapacitance contribution is dominant over the double layer capacitance due to the high surface area and the porous nature of the material.

### **6.3.2. Electrochemical impedance spectroscopy**

In order to investigate the electrochemical characteristics of the supercapacitor electrodes | electrolyte interface in a quantitative manner, ac impedance spectroscopic measurements were performed. Figures 5 (a) and (b) show the respective Nyquist plots of symmetric and asymmetric supercapacitor cell assemblies based on the high surface area porous nickel and activated

carbon in 6M KOH aqueous solution. Inset shows the expanded high frequency region of the same plot.

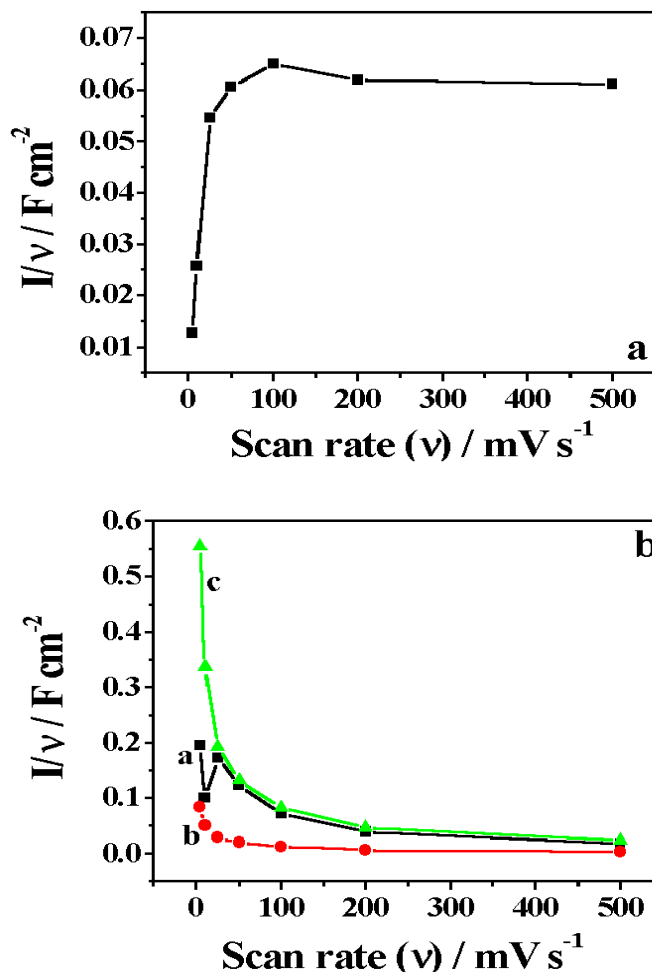


Figure 4: Variation of  $I/v$  with different scan rates used for the capacitance measurement using cyclic voltammetry for (a) Symmetric supercapacitor of high surface area porous nickel (Porous Ni| KOH |Porous Ni). (b) Similar plots for the other cell assemblies namely (a) Asymmetric supercapacitor based on the porous nickel electrode (Porous Ni| KOH |Activated carbon). (b) Symmetric supercapacitor (NiO| KOH |NiO) and (c) Asymmetric supercapacitor (NiO| KOH |Activated carbon) based on nickel oxide electrode.

It can be seen from the figures 5 (a) and (b) that the cell shows a depressed semicircle at high frequency region and a straight line at lower frequency region. This implies that the supercapacitors show a blocking behaviour at high frequencies and capacitive behaviour at low frequencies. The impedance plots obtained in this case are similar to that of transmission line model (TLM) for the porous electrodes proposed by Conway [8,39] for the case of under potential deposition with continuous reaction. The TLM consists of a parallel combination of R and C elements interconnected with the pore resistance element,  $R_p$ . In our case, the contribution from pseudocapacitance due to the redox reaction of nickel hydride is dominant at this potential for the porous nickel electrodes, which gives an additional pseudocapacitance element ( $C_\phi$ ). The phase angle values close to  $65^\circ$  and  $70^\circ$  are obtained for the symmetric (Porous Ni| KOH |Porous Ni) and asymmetric (Porous Ni| KOH |Activated carbon) supercapacitors respectively, indicating a dominant capacitive behaviour.

Figures 6 (a) and (b) show the respective Nyquist plots of symmetric and asymmetric supercapacitors based on NiO electrode in 6M KOH aqueous solution. The insets of the figures show an expanded high frequency region. It can be inferred from the plots that the supercapacitors show a very small kinetic arc at high frequencies implying the charge transfer controlled regime and a straight line at low frequencies indicating the capacitive regime. A phase angle of  $65^\circ$  and  $77^\circ$  obtained for the respective symmetric and asymmetric supercapacitors based on NiO electrodes, imply that the material is suitable for the fabrication of low leakage capacitors.

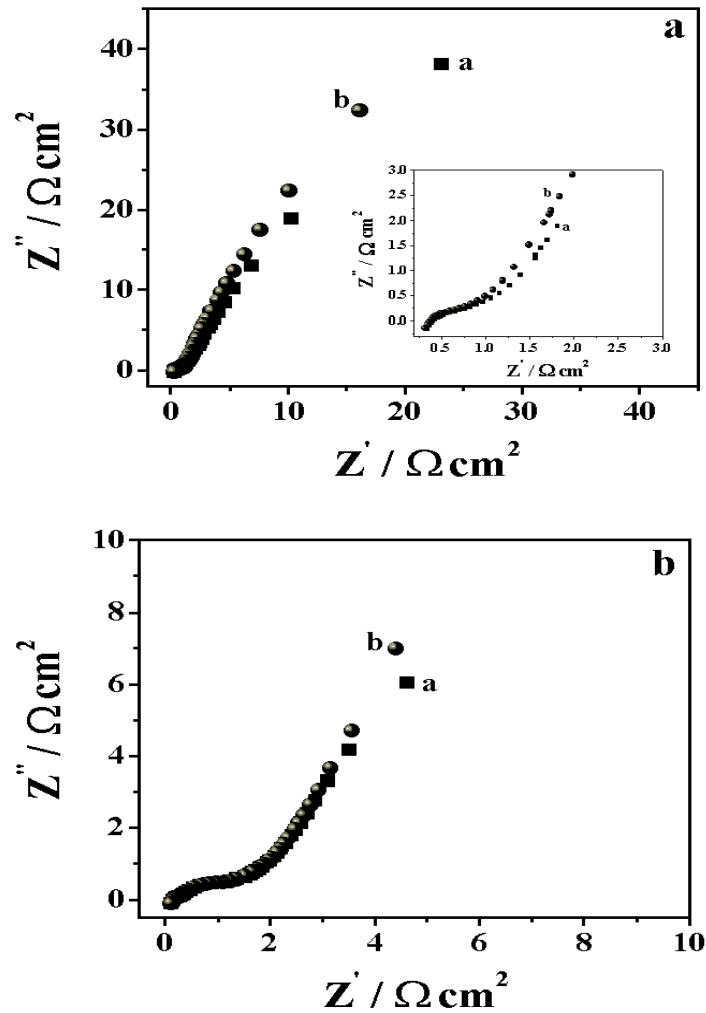


Figure 5: Nyquist plots using high surface area porous Ni as an electrode material for (a) Symmetric supercapacitor (Porous Ni| KOH |Porous Ni) at two different dc potentials of a)  $-1.0$  V and b)  $-0.9$  V and for (b) Asymmetric supercapacitor (Porous Ni| KOH |Activated carbon) at two different dc potentials of a)  $-1.0$  V and b)  $-0.9$  V in 6M KOH aqueous solution. Inset shows the expanded high frequency region of the same plot.

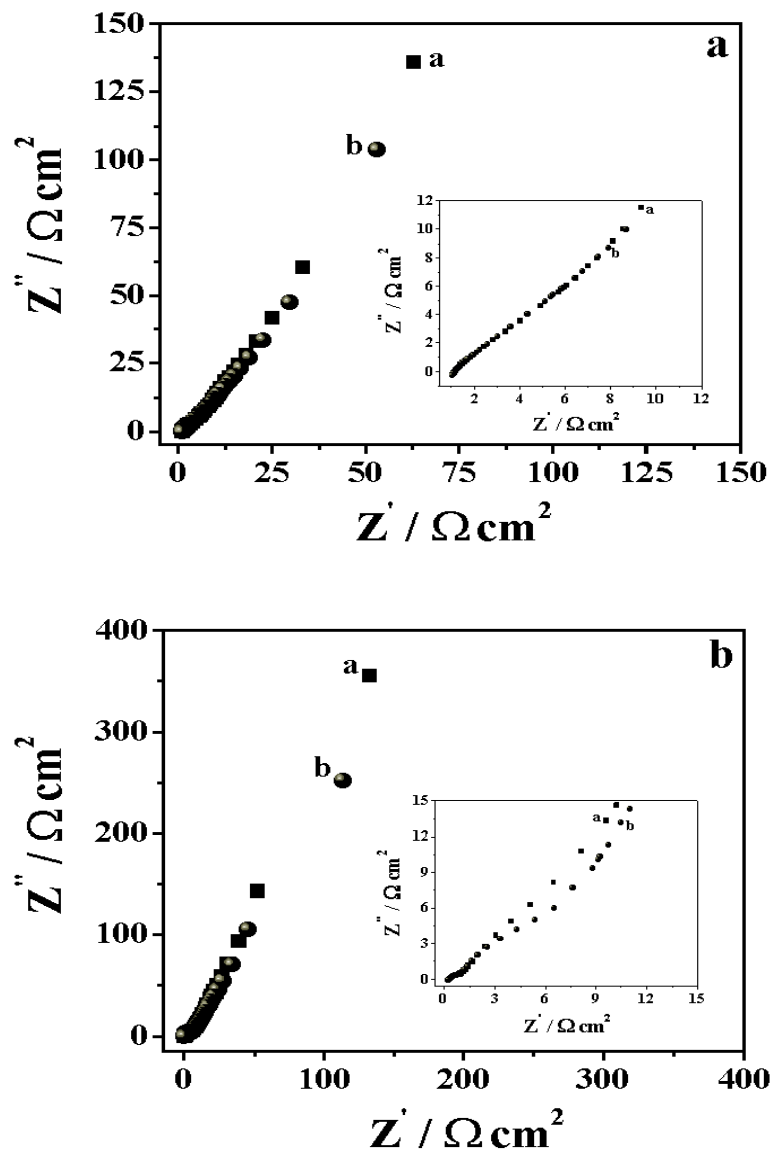


Figure 6: Typical impedance (Nyquist) plots using NiO obtained from the porous Ni as an electrode material in 6M KOH aqueous solution for (a) Symmetric supercapacitor (NiO| KOH |NiO) at dc potentials of a) 0 V and b) 0.1 V and (b) Asymmetric supercapacitor (NiO| KOH |Activated carbon) at dc potentials of a) 0 V and b) 0.1 V. Insets show the zoomed portion of the same plot at high frequency region.

In general, a supercapacitor behaves as a pure resistor at high frequencies and as a capacitor at low frequencies. In the mid frequency range, it behaves as a combination of resistor and capacitor, where the electrode porosity and thickness of electroactive materials play a vital role in the determination of capacitance values. This is in conformity with the transmission line model. The above-mentioned effect shifts the low frequency capacitive behaviour towards the more resistive values along the real axis, from which equivalent distributed resistance (EDR) arising due to the porous nature of the electrode material can be determined. From the high frequency intercept of the semicircle, the equivalent series resistance (ESR) can be calculated. In the present study, ESR value is more due to the additional EDR arising from the resistance offered by the diffusion of ions through the pores, which contributes to the overall resistance value. There have been several models proposed to explain the frequency behaviour of supercapacitor materials such as the transmission line model [40], and the models based on size and shape of the pores (pore size distribution model) [41,42]. In our case, we have followed the analysis of complex capacitance and complex power method [43,44], which is a simple procedure to investigate the utility of the supercapacitors using their impedance data.

### **6.3.3. Complex capacitance and complex power analysis**

The relaxation time constant ( $\tau_0$ ), which is also known as dielectric relaxation time of the supercapacitor [45], corresponds to the figure of merit of the supercapacitor [46]. This parameter represents one of its discharge characteristics. Several other workers used the analysis of complex capacitance and complex power method to investigate the various supercapacitor cell assemblies using their impedance data [43,44].

The complex capacitance is expressed as follows,

$$C(\omega) = C'(\omega) - j C''(\omega) \quad (1)$$

where  $C'(\omega)$  is the real part of the complex capacitance and  $C''(\omega)$  is the imaginary part of the complex capacitance,  $C(\omega)$  and they are given by,

$$C'(\omega) = - Z''(\omega) / \{ \omega |Z(\omega)|^2 \} \quad (2)$$

and

$$C''(\omega) = Z'(\omega) / \{ \omega |Z(\omega)|^2 \} \quad (3)$$

where  $Z'(\omega)$  and  $Z''(\omega)$  are the respective real and imaginary parts of the complex impedance,  $Z(\omega)$ .  $\omega$  is the angular frequency and it is given by  $\omega = 2\pi f$ .

At low frequency,  $C'(\omega)$  corresponds to the capacitance of the electrode material and  $C''(\omega)$  corresponds to the energy dissipation by an irreversible process that leads to a hysteresis [43].

The value of complex power can be expressed as,

$$S(\omega) = P(\omega) + j Q(\omega) \quad (4)$$

where the real part of the complex power,  $P(\omega)$  is called as the active power and  $Q(\omega)$ , the imaginary part is known as the reactive power, which are given by,

$$P(\omega) = \omega C''(\omega) | \Delta V_{\text{rms}} |^2 \quad (5)$$

and

$$Q(\omega) = - \omega C'(\omega) | \Delta V_{\text{rms}} |^2 \quad (6)$$

where  $| \Delta V_{\text{rms}} |^2 = \Delta V_{\text{max}} / \sqrt{2}$  with  $V_{\text{max}}$  being the maximal amplitude of the ac signal.

The relaxation time constant,  $\tau_0 (=1/2\pi f_0)$  can be calculated from the plots of  $C'(\omega)$  vs. frequency and  $C''(\omega)$  vs. frequency. The real part of the

complex capacitance,  $C'(\omega)$  decreases asymptotically with frequency. This is characteristic of the electrode structure and electrode | electrolyte interface. From the frequency corresponding to the half of the maximum value of  $C'(\omega)$ , the relaxation time constant ( $\tau_0$ ) can be determined. The change of imaginary part of the complex capacitance,  $C''(\omega)$  with frequency goes through a maximum at a frequency,  $f_0$ , from which the value of  $\tau_0$  can be calculated. Figures 7 (a-d) show the variation of  $C''(\omega)$  with frequency for the symmetric and asymmetric supercapacitor cell assemblies studied in this work. The plots show a characteristic hysteresis for all the supercapacitor cell assemblies investigated. It can be noted that the symmetric and asymmetric cell assemblies based on nickel oxide supercapacitors show a clear peak formation, while the cell assemblies based on the porous nickel electrodes have not reached the maximum even at the lowest frequency used in this study.

The plots of normalized power with the frequency shown in figures 8 and 9 represent the relaxation time constants for the respective supercapacitor cell assemblies. The power dissipated into the system can be analyzed from the normalized active power denoted by  $|P|/|S|$ . At high frequency, when the supercapacitor behaves like a pure resistor, all the power is dissipated into the system ( $P=100\%$ ). However, no power is dissipated into a pure capacitance at low frequency. Infact, the values of  $|P|/|S|$  and  $|Q|/|S|$  show opposite trends with frequency as can be seen from the figures 8 and 9. The crossing of two plots occurs at a frequency  $f_0$ , known as resonance frequency, from which the relaxation time constant,  $\tau_0$  ( $=1/2\pi f_0$ ), can be determined explicitly. This time constant,  $\tau_0$  corresponds to a phase angle of  $45^\circ$  and it represents the transition of electrochemical capacitor from a purely resistive to a purely capacitive behaviour. For a frequency,  $f > 1/\tau_0$ , it acts as a pure resistor and for  $f < 1/\tau_0$ , it

behaves as a pure capacitor. In our work, we have used the complex power method for the analysis, which is the most appropriate one for evaluating the figure of merit of the supercapacitor cell assemblies.

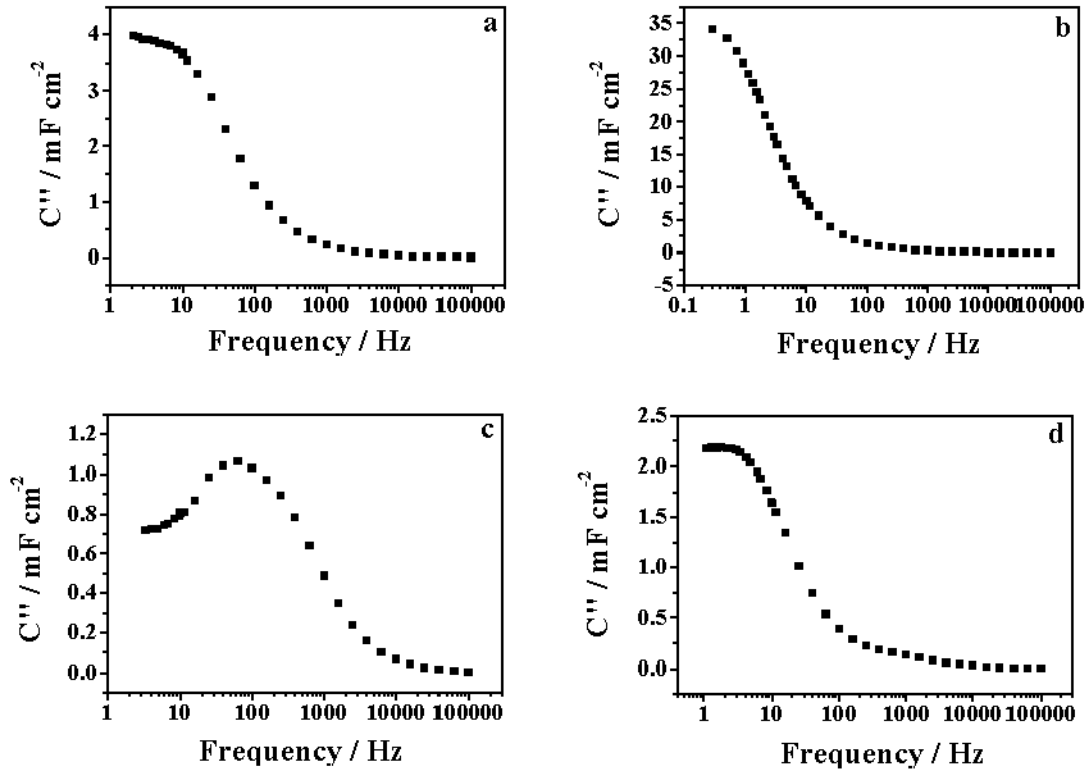


Figure 7: The plots of imaginary part of the complex capacitance [ $C''(\omega)$ ] with the frequency (in logarithmic scale) for, (a) Symmetric supercapacitor (Porous Ni/ KOH /Porous Ni) and (b) Asymmetric supercapacitor (Porous Ni/ KOH /Activated carbon) based on the high surface area porous nickel electrode. (c) Symmetric supercapacitor (NiO/ KOH /NiO) and (d) Asymmetric supercapacitor (NiO/ KOH /Activated carbon) based on the nickel oxide electrode.

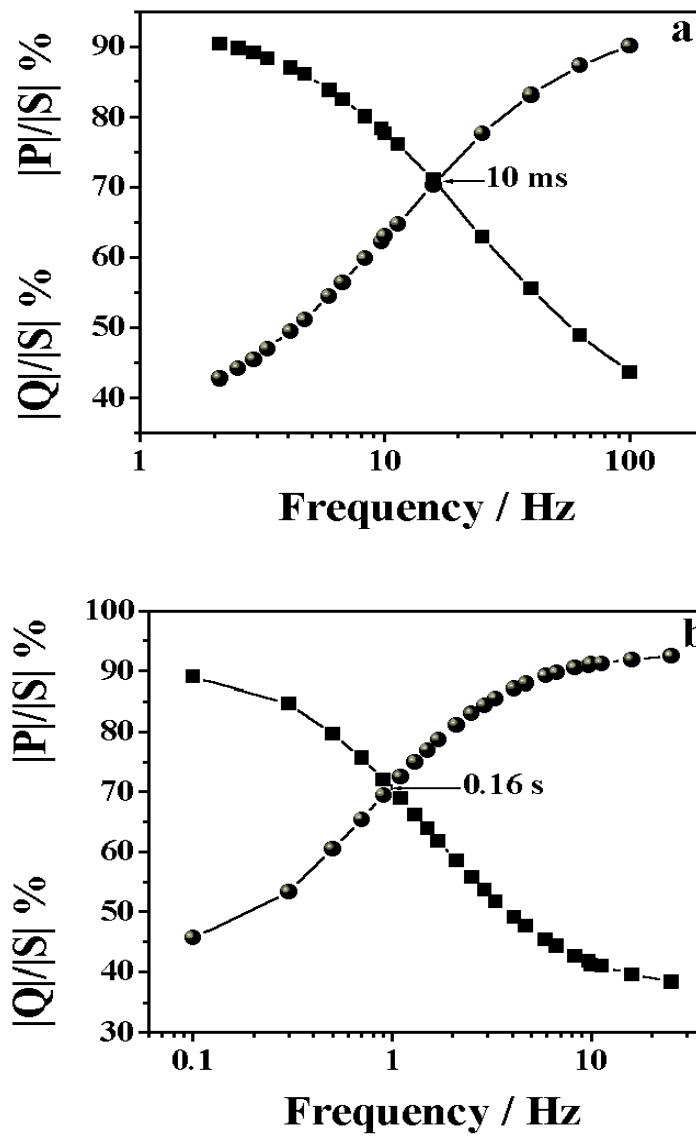


Figure 8: Plots of normalized active power,  $|P|/|S|$  and reactive power  $|Q|/|S|$  vs. frequency (in logarithmic scale) for (a) Symmetric and (b) Asymmetric supercapacitor cell assemblies using the high surface area porous Ni as an electrode material.

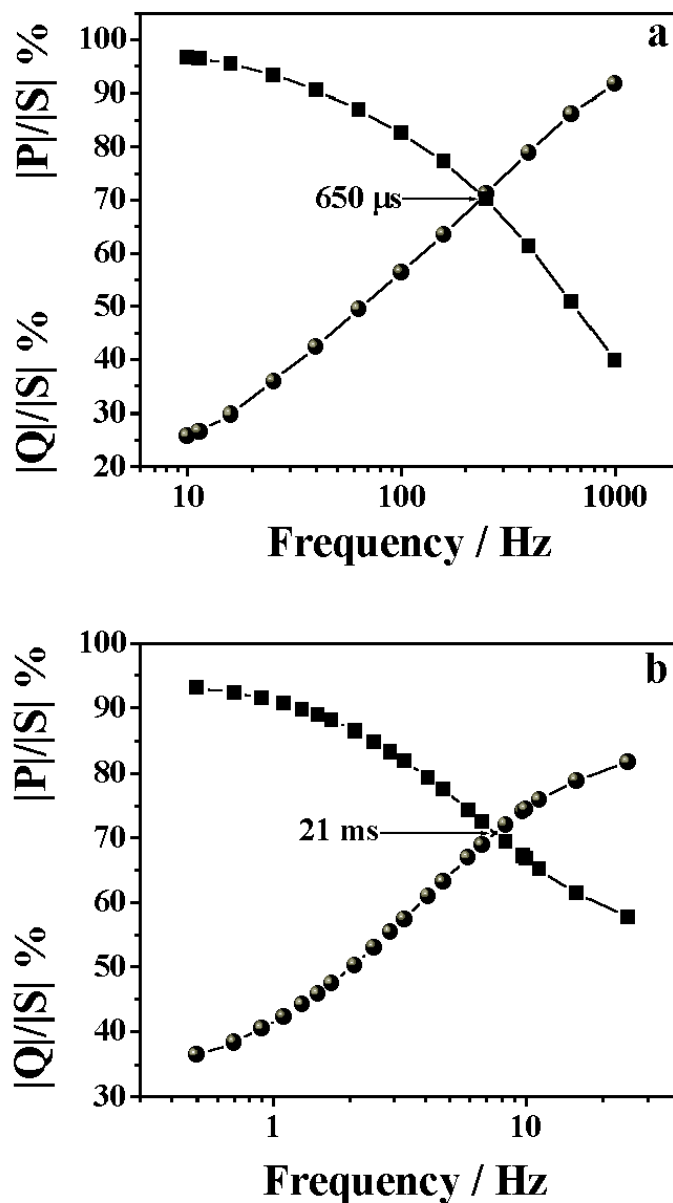


Figure 9: Plots of normalized active power,  $|P|/|S|$  and reactive power  $|Q|/|S|$  vs. frequency (in logarithmic scale) for (a) Symmetric and (b) Asymmetric supercapacitor cell assemblies using NiO electrodes obtained from the electrochemical oxidation of porous Ni as an electrode material.

Figures 8 (a) and (b) show the plots of  $|P|/|S|$  and  $|Q|/|S|$  of the complex power vs. frequency (in logarithmic scale) for the respective symmetric and asymmetric supercapacitors based on the high surface area porous nickel electrode. These parameters show the expected trends as discussed above. From the crossing of two plots at a frequency,  $f_0$ , the value of  $\tau_0$  has been determined. A value of 10ms and 0.16s have been calculated for the respective symmetric (Porous Ni| KOH |Porous Ni) and asymmetric (Porous Ni| KOH |Activated carbon) supercapacitors indicating that the cell based on the symmetric system is able to deliver its stored energy almost ten times faster at a high power. Figures 9 (a) and (b) show the plots of  $|P|/|S|$  and  $|Q|/|S|$  of the complex power vs. frequency (in logarithmic scale) for the respective symmetric and asymmetric supercapacitor cell assemblies based on NiO electrode, obtained by the electrochemical oxidation of porous Ni electrode. The relaxation time constant ( $\tau_0$ ) values of 650 $\mu$ s and 21ms are determined for the symmetric (NiO| KOH |NiO) and asymmetric (NiO| KOH |Activated carbon) supercapacitor cell assemblies respectively. By comparing the figures 8 and 9 and from the measured relaxation time constant values, it is evident that the response time is faster for the NiO supercapacitors than the porous Ni electrode system, even though the specific capacitance value is higher for the latter. In addition, the symmetric cell assembly provides the faster delivery of stored energy at a much higher power when compared to the asymmetric cell assembly.

#### **6.3.4. Charge-Discharge profile analysis**

In order to evaluate the charge storage capacity, durability of cycle lifetime and to determine various electrical parameters, the galvanostatic charge-discharge analysis of the supercapacitor cell assemblies were performed at two different current densities namely 1 mA/cm<sup>2</sup> and 4 mA/cm<sup>2</sup>. Several

electrical parameters such as specific capacitance (SC), specific power (SP) and specific energy (SE) are calculated using the following relationships [6],

$$SC = [I \times t] / [V \times m] \quad (7)$$

$$SP = [I \times V] / m \quad (8)$$

$$SE = [I \times t \times V] / m \quad (9)$$

where SC is specific capacitance in F/g, SP is specific power in W/g and SE is specific energy in Wh/g. The above-mentioned expressions show the discharge current (I) in amperes, voltage range (V) in volts, discharge time (t) in seconds and mass of the electroactive material (m) in grams. The coulombic efficiency of supercapacitors is calculated using the following equation,

$$\eta = [t_D / t_C] \times 100 \quad (10)$$

where  $t_C$  and  $t_D$  represent the time of charging and discharging respectively.

Figures 10 (a) and (b) show the typical charge-discharge profiles of the respective symmetric and asymmetric supercapacitor cell assemblies using the high surface area porous nickel electrodes in 6M KOH aqueous solution. We have used a voltage range of 0 to 1V in order to evaluate the performance of these supercapacitors at higher voltages. It can be seen that the charge-discharge profiles deviate from the typical linear variation of voltage with time normally exhibited by a purely electrochemical double layer capacitor (EDLC). The observed non-linearity in our case can be explained as due to the pseudocapacitance arising out of the redox reaction at this voltage range. It can also be noted that the charging-discharging times are almost the same. For symmetric supercapacitor (Porous Ni| KOH |Porous Ni), a specific capacitance of 23 F/g is obtained at 4 mA/cm<sup>2</sup> with a specific power of 1.23 W/g and a specific energy of 23.31 kWh/kg. The specific capacitance value decreases to 50% after 500 cycles. The coulombic efficiency ranges from 0.93 to 0.99.

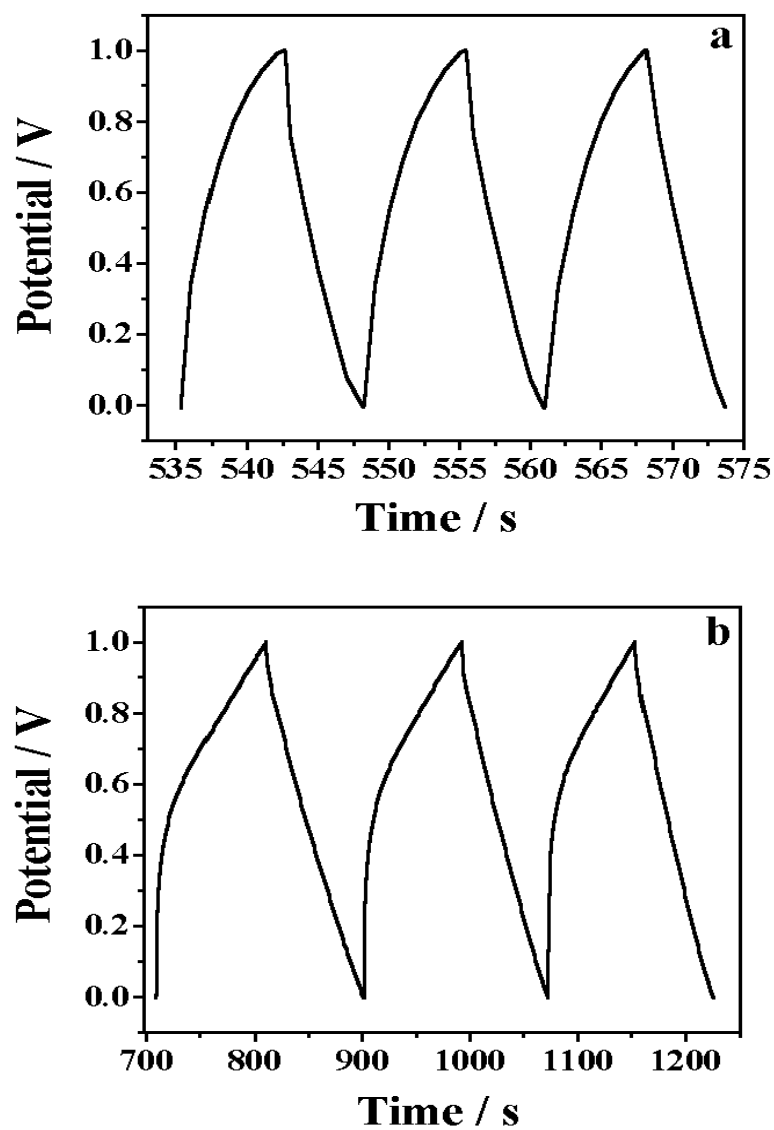


Figure 10: Representative galvanostatic charge-discharge curves for the respective devices of (a) Symmetric (Porous Ni| KOH |Porous Ni) and (b) Asymmetric (Porous Ni| KOH |Activated carbon) supercapacitor cell assemblies based on the high surface area porous Ni as an electrode material in 6M KOH aqueous solution.

There is a large voltage drop at the beginning of the discharge curve, which is attributed to the resistance arising out of the porous nature of the electrode. For the asymmetric supercapacitor (Porous Ni| KOH |Activated carbon), a specific capacitance of 30 F/g is obtained at 1 mA/cm<sup>2</sup> current density with a specific power of 330 W/kg and a specific energy of 28.88 Wh/g. In this case also the specific capacitance value decreases to 50% of its original value after 500 cycles. The coulombic efficiency value ranges from 0.91 to 0.97. However, there is no significant voltage drop during the initial stage of the discharge process. Here the variation of voltage with respect to time is again not linear due to the porous nature of the electrode materials, which conforms to the proposed model of Conway and Pell [39]. The equivalent series resistance (ESR) value increases marginally with the number of cycles when activated carbon was used as the negative electrode in the asymmetric supercapacitor cell assemblies.

The high surface area porous nickel was electrochemically oxidized to obtain its corresponding NiO as discussed earlier. Figures 11 (a) and (b) show the representative charge-discharge profiles of both the symmetric and asymmetric supercapacitor cell assemblies based on NiO electrode in 6M KOH aqueous solution respectively. It can be seen that the symmetric NiO supercapacitor cell assembly (Fig. 11(a)), exhibits a non-linear charge-discharge profile. On the other hand, the asymmetric cell assembly (Fig. 11(b)) shows a perfect linear characteristic, implying the formation of a good electrode | electrolyte interface with a well-defined conductivity. In addition, no ohmic drop is observed in the case of asymmetric supercapacitor and not quite significant ohmic drop in the case of symmetric cell assembly. We have employed two different current densities for the measurements as mentioned earlier, in which the activated carbon was used as a negative electrode.

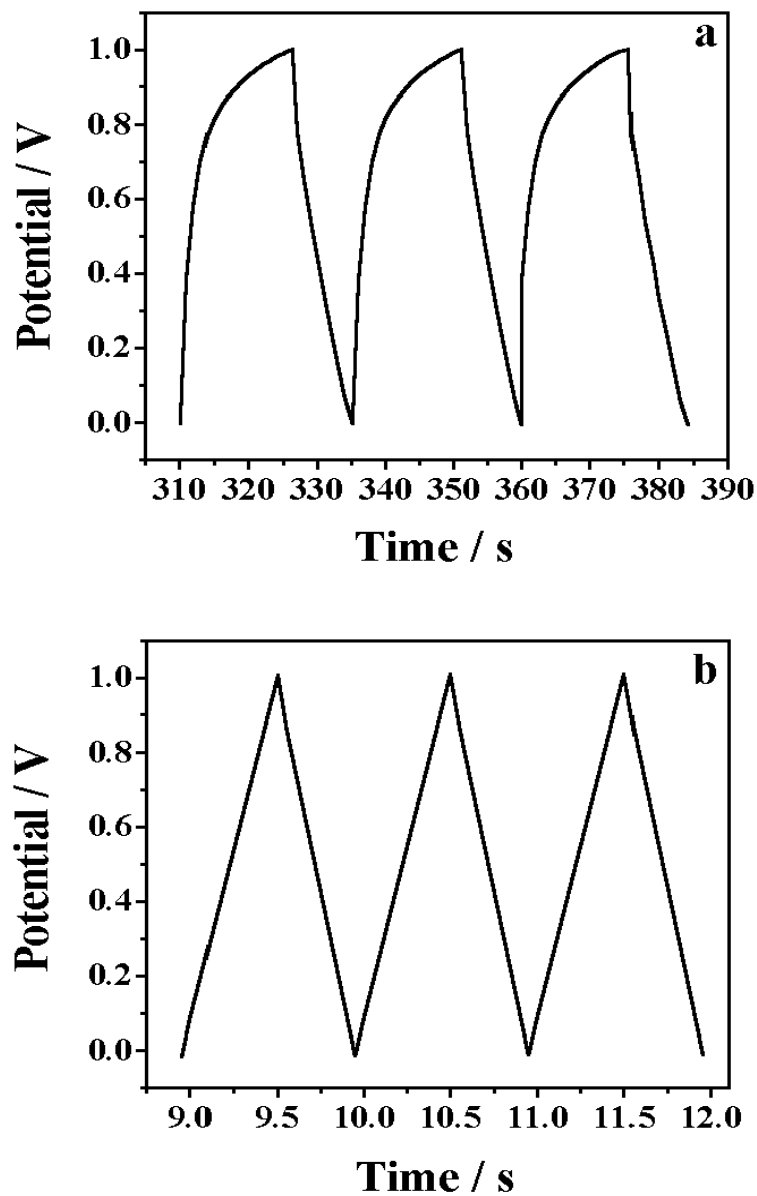


Figure 11: Typical galvanostatic charge-discharge profiles of (a) Symmetric (NiO| KOH | NiO) and (b) Asymmetric (NiO| KOH | Activated carbon) supercapacitor cell assemblies based on NiO as an electrode in 6M KOH aqueous solution respectively.

For the symmetric supercapacitor (NiO| KOH |NiO), a specific capacitance of 37 F/g is obtained at a constant current density of 4 mA/cm<sup>2</sup> with a specific power of 1.23 W/g and a specific energy of 37 Wh/g. Infact the specific capacitance value decreases to a large extent with the number of cycles while the ESR value increases marginally. The coulombic efficiency of the cell ranges from 0.85 to 0.97. For asymmetric supercapacitor (NiO| KOH |Activated carbon), a specific capacitance of 40 F/g at a constant current density of 1 mA/cm<sup>2</sup> with a specific power of 330 W/kg and a specific energy of 35 Wh/g is obtained. The coulombic efficiency of the cell assembly ranges from 0.80 to 0.90. It can be seen that the specific capacitance values measured from the charge-discharge analysis described above for the different supercapacitor cell assemblies are always higher than the corresponding values determined from cyclic voltammetry shown in Table 1 and 2. This can be attributed to the different potential ranges used for the capacitance measurement in these two methods. The larger value in the case of charge-discharge studies arises from the enhanced pseudocapacitance contribution to the total measured capacitance.

Usually, the ESR values for the supercapacitors lie in the range of a few hundreds of milliohms, which arises mainly from the contact and electrolytic resistances. In the case of porous electrodes, the contribution from equivalent distributed resistance (EDR) may also add to the measured ESR value. In the present study, the symmetric supercapacitor (Porous Ni| KOH |Porous Ni) based on the high surface area porous Ni alone shows a higher ESR value ranging from ~10Ω-20Ω, compared to ~1Ω-3Ω of all the other supercapacitor cell assemblies investigated in this work. The fact that the asymmetric supercapacitor (NiO| KOH |Activated carbon) cell assembly based on NiO electrode shows almost no voltage drop rules out the contribution from the contact resistance. Obviously, the ESR contribution in other cell assemblies

arises from the contact resistance of the respective cell assembly. The higher ESR value in the case of symmetric porous nickel supercapacitor can be attributed to the diffusional resistance (EDR) of the electrolyte inside the pores [47]. We have earlier described about a flooded pear shaped pore model [28] for the porous nickel material obtained using template electrodeposition (See chapter 3 for further details). This particular pore geometry of the porous nickel makes it difficult for a free flow of ions, which leads to a large increase in the resistance value. The fact that the asymmetric supercapacitor cell assembly based on NiO electrode has a very negligible ESR value implies that the geometry of the pores is altered during the process of electrochemical oxidation. It is felt that this behaviour facilitates better ionic flow within the pores. In spite of the higher ESR and lower specific capacitance values, these supercapacitors have fast response time, which are well suited for applications in short duration pulse devices.

Several parameters determined from the charge-discharge analysis of symmetric and asymmetric supercapacitor cell assemblies based on the high surface area porous nickel and its corresponding nickel oxide electrodes are shown in Table 3. It can be seen from the table that the double layer capacitance and its corresponding specific capacitance values are not very high, as compared to the reported specific capacitance values. The coulombic efficiency of all the supercapacitor cell assemblies is high. Even though the ESR values of the supercapacitors of porous Ni and its corresponding NiO electrodes are on the higher side, the response time of these supercapacitors are quite fast, making it possible for the potential applications in short duration pulse devices. From these experiments, it is clear that the high surface area porous Ni obtained from template electrodeposition and its corresponding NiO electrode obtained

by electrochemical oxidation method are the promising electrode materials for supercapacitor applications.

**Table-3**

Several parameters such as double layer capacitance, specific capacitance, specific energy, specific power, coulombic efficiency, response time, ESR values and lifetime determined from the charge-discharge analysis of the symmetric and asymmetric supercapacitor cell assemblies based on the high surface area porous Ni and nickel oxide electrodes.

Parameters	Porous nickel		Nickel oxide (NiO)	
	Symmetric	Hybrid	Symmetric	Hybrid
<b>Double layer capacitance (mF/cm<sup>2</sup>)</b>	<b>66</b>	<b>250</b>	<b>15</b>	<b>100</b>
<b>Specific capacitance (F/g)</b>	<b>22</b>	<b>84</b>	<b>5</b>	<b>57</b>
<b>Specific energy (Wh/g)</b>	<b>23.31</b>	<b>28.88</b>	<b>37</b>	<b>35</b>
<b>Specific power (W/g)</b>	<b>1.23</b>	<b>0.33</b>	<b>1.23</b>	<b>0.33</b>
<b>Coulombic efficiency (%)</b>	<b>99</b>	<b>97</b>	<b>97</b>	<b>90</b>
<b>Response time (ms)</b>	<b>10</b>	<b>160</b>	<b>0.65</b>	<b>21</b>
<b>ESR values (ohms)</b>	<b>18</b>	<b>3</b>	<b>2</b>	<b>-----</b>
<b>Lifetime (no. of cycles)</b>	<b>500</b>	<b>500</b>	<b>500</b>	<b>500</b>

## **II. EVALUATION AS A HYDROGEN EVOLVING CATHODE**

### **6.4. Introduction to hydrogen evolving cathodes**

Recently, there is an increasing attention that has been paid to the production of hydrogen to use as the basis of an energy system essentially to replace the carbon-based fossil fuels, mainly for two reasons namely the global warming and depletion of energy resources. Hydrogen is very much useful for reducing emissions from the vehicle, since it reacts with oxygen and produces only water as the reaction product. It can be used to provide electricity and heat either through use in fuel cell or combustion. A fuel cell generates electricity by combining hydrogen with oxygen from air and produces water as the by-product. Unlike the other resources such as oil, gas and coal, hydrogen does not exist in large quantities in nature in a useful form. It has to be produced using several methods and stored in a proper condition. Hydrogen can be produced using a number of different routes such as from hydrocarbons (oil, coal and natural gas), from biomass and wastes and by electrolysis of water.

Today, nearly more than half of the hydrogen used is produced mainly from fossil fuels and natural gas using steam-reforming process. The other alternative cheap method of producing hydrogen is the electrolysis of water. Until 1950's this method is very popular and extensively used for the generation of hydrogen. This method involves the usage of an electric current to split water into hydrogen and oxygen and it provides only a small volume of highly pure hydrogen. However, there is a renewed interest in the use of electrolysis for producing hydrogen to be used as a fuel or for energy storage. The hydrogen evolving cathodes are useful in industrial electrochemical processes such as the chloralkali process and the electrolysis of alkaline water. Cathodic hydrogen evolution is mainly based on the platinum metals such as Pt and Ru and to a lesser extent by iron, cobalt and nickel [48]. In the transition

metal series, only nickel (Ni) is stable in alkaline medium at the hydrogen equilibrium potential [49]. To compensate for the lower electrocatalytic activity and simultaneously to take the advantage of relatively lower price of nickel as compared to platinum metals, Raney nickel was used as an efficient cathodic hydrogen evolution catalyst in alkaline water and chloralkali electrolysis. The use of Raney nickel coatings was triggered by the successful application of this in fuel cells by Justi and Winsel [50].

Preparation and study of high true surface area nickel and its alloys are of interest as they are used as hydrogen evolving cathodes in industry for various electrochemical processes. Simpraga et al. obtained a very high roughness factor value of the order of 2800 for Ni-Fe composite electrodes prepared by a simple electrochemical co-deposition process [51]. Rausch and Wendt characterized the high surface area sintered Ni and Raney Ni for their electrocatalytic properties using Tafel plots and electrochemical impedance spectroscopy [52]. Brown and Sotiropoulos reported the preparation of a highly porous large surface area nickel deposit from a high internal phase emulsion (HIPE) template [30]. This is basically a water-in-oil emulsion where water content exceeds 75% v/v. They obtained a highly porous deposit having irregular structure that shows relatively low overpotential for hydrogen evolution reaction. It was shown that the materials prepared by HIPE template deposition technique are more effective than sintered nickel in its electrocatalytic activity.

In this work, we have evaluated the high surface area porous nickel obtained using template electrodeposition (See chapter 3 for further details) as a potential material for the hydrogen evolution catalyst and compared with the other existing nickel electrocatalysts. We have used Tafel plot analysis for the

study of hydrogen evolution reaction (her) on the high surface area porous Ni deposit and its evaluation as an electrocatalyst.

## 6.5. Experimental section

Electrochemical characterization and evaluation of the deposit was carried out in an all glass three-electrode electrochemical cell. A platinum foil of large surface area was used as a counter electrode and a saturated calomel electrode (SCE), which was kept in a separate compartment was used as a reference electrode. The true surface area of the template deposited porous nickel material was determined in terms of the roughness factor using cyclic voltammetry (See chapter 3 for a detailed procedure). The roughness factor of the porous nickel electrode is determined to be about 3620, a highest value reported for any electrodeposited nickel [28] in the literature. This material has been evaluated as a potential candidate for hydrogen evolution catalyst using Tafel plot analysis by studying hydrogen evolution reaction on this deposit. The chronoamperometric experiments for hydrogen evolution reaction were conducted by the application of a series of potential steps of 10-20 mV amplitude for a duration of 20s between  $-1.1$  V to  $-1.3$  V vs. SCE in a cell containing a separate compartment for the reference electrode. The potential data were corrected for ohmic drop due to the solution resistance  $R_u$  that has been determined using current interruption technique. Finally, we have compared the current density values obtained for this high surface area porous nickel electrode with the other existing Ni electrocatalyst such as sintered nickel, Raney Ni and a porous Ni obtained from High Internal Phase Emulsion (HIPE) template in terms of both the geometric area of the material and mass of the electrodeposited material.

## 6.6. Results and discussion

### 6.6.1. Tafel plot analysis

The utility of high surface area porous nickel (obtained using template electrodeposition) as hydrogen evolving cathodes has been evaluated electrochemically in 0.5M NaOH aqueous solution. The steady state overpotential ( $\eta$ ) – current density ( $i$ ) data were obtained using chronoamperometry experiments [30,53]. The protocol consisted of first keeping the electrode at a potential of -1.6 V vs. SCE for 5 minutes in the hydrogen evolution region followed by applying a pulse to -1.02 V vs. SCE for 60s in order to oxidize any hydrides that has been formed. Finally the desired potential was applied starting from -1.05 V vs. SCE to collect chronoamperometry data. The steady state current is measured at the end of 20s. Figure 12 shows the linear region of  $\eta$  versus  $\log i$  plots for the smooth as well as the porous nickel electrodes. A Tafel slope of around 120 mV dec<sup>-1</sup> was obtained for both the smooth nickel and the electrodeposited high surface area porous nickel electrodes. This indicates that the rate-determining step for hydrogen evolution reaction is the same in both the cases following the Volmer-Heyrovski mechanism [54-57].

It can be seen from the figure 4 that there is an increase in current density by more than 200 times due to hydrogen evolution reaction on the porous nickel deposit when compared to smooth nickel electrode. This increase in current density essentially arises from the increase in surface area of the porous nickel material as confirmed by the cyclic voltammetric and electrochemical impedance spectroscopic measurements that have been explained elaborately in chapter 3. A large current density arises due to improved accessibility of the electrolyte to the interior portion of the pores. This is a measure of the electrolytically ‘wetable area’ during the hydrogen

evolution reaction. In this case, we have obtained a higher current density of  $200 \text{ mA/cm}^2$  at a relatively lower overpotential of about 260 mV.

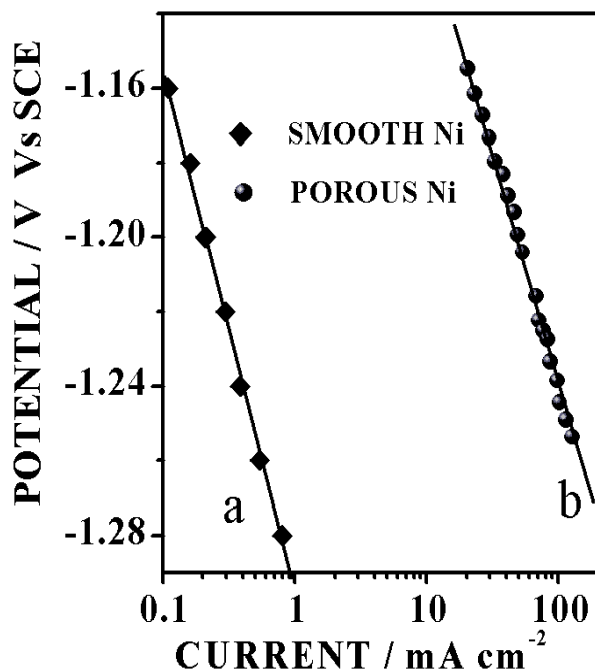


Figure 12: Logarithmic current density vs. potential curves for hydrogen evolution reaction in 0.5M NaOH aqueous solution for, (a) smooth nickel electrode and (b) as plated porous nickel electrode prepared using template electrodeposition.

### 6.6.2. Comparison of current-potential characteristics of the porous Ni with other hydrogen evolving Ni cathodes

We have compared the effectiveness of the porous Ni electrodeposited material obtained using template electrodeposition to be a hydrogen-evolving cathode with other existing Ni electrocatalytic materials reported in literature. We have obtained the required data for Raney nickel and sintered Ni electrodes from the work of Rausch et al. [52] and for the high internal phase emulsion

(HIPE) template electrodeposited nickel material from Brown et al. [30]. Figures 13 (a) and (b) show the plots of overpotential vs. current density with respect to substrate geometric area and mass of deposited Ni for different electrodes respectively. It can be noted from the figure 13 (a) that the porous Ni electrode has the highest current density per unit geometric area among all the other Ni electrodes reported earlier. This is also seen from the data shown in Table 4, where the ratio of the current densities as reported in literature for sintered Ni, Raney Ni and HIPE template Ni are compared.

**Table-4**

The relative effective nickel electrode surface area as measured by the ratio of hydrogen evolution current densities of different nickel electrodes and a smooth reference nickel surface.

<b>Sample</b>	<b>Surface area measured using current-potential curves</b>
<b>Smooth nickel</b>	<b>1</b>
<b>Sintered nickel</b>	<b>30</b>
<b>Raney nickel</b>	<b>34 (at 1 mA/cm<sup>2</sup>) 1000 (at 1 A/cm<sup>2</sup>)</b>
<b>HIPE template nickel</b>	<b>65*</b>
<b>Porous Ni (our work)</b>	<b>230</b>

\* Value extracted from Figure 4 (a) of reference [30].

It can be seen that the relative ratio of 230 obtained from the current densities of porous Ni and smooth Ni electrodes is almost 28% of the electroactive area showing that a significant portion of the surface is utilized for

the hydrogen evolution reaction. The fraction of the available area utilized for the hydrogen evolution reaction is better than that of sintered Ni and Raney Ni electrodes.

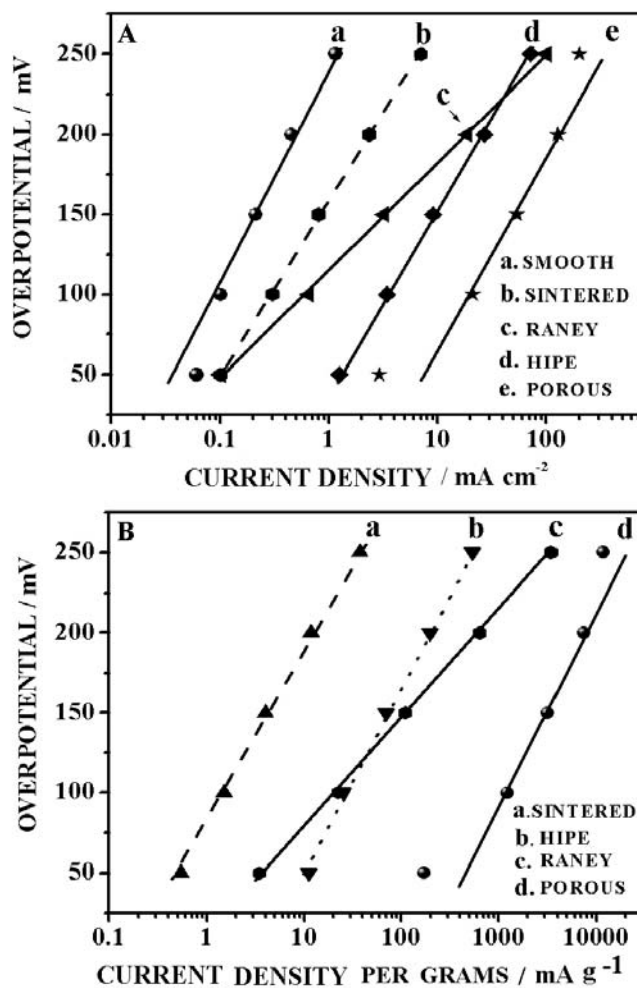


Figure 13: Plots of (A) logarithmic current density (per substrate geometric area) vs. overpotential curves and (B) logarithmic current density (per mass of deposited Ni) vs. overpotential curves for different Ni electrodes in alkaline medium. The data points of (b) and (c) of figure A are obtained from Ref. [52] and (d) from ref. [30]. Similarly the data points of (a) and (c) are obtained from Ref. [52] (mass of sintered Ni = 125 mg/cm<sup>2</sup>; porosity = 0.6 and mass of Raney Ni = 29 mg/cm<sup>2</sup>; porosity = 0.35) and (b) from Ref. [30].

However, it is very much less than that of HIPE template deposited Ni material where, as can be seen from the table 4, almost all the available electroactive area has been utilized for the hydrogen evolution reaction. This may be due to the more open architecture of the pores present in the HIPE template deposit [30]. Figure 13 (b) shows the plots of overpotential vs. current density per gram of deposited Ni for different Ni electrode materials. It can be seen that the porous Ni material prepared using the hexagonal liquid crystalline template (present work) shows the most effective utilization of the available mass of deposited Ni among all the other electrocatalytic materials compared in this work. The effectiveness of the material arises essentially due to a very large electroactive surface area, which is also quite well accessed by the electrolyte (as described in chapter 3 based on the results of double layer capacitance measurement). Based on these results, it can be concluded that the high surface area porous nickel prepared by template electrodeposition using a hexagonal liquid crystalline phase as a template can be a potential source of hydrogen evolving cathode in electrocatalysis.

## **6.7. Conclusions**

In this chapter, we have shown that the high surface area porous nickel obtained from template electrodeposition can be a possible source of applications in supercapacitors as an electrode material and as a hydrogen-evolving cathode in electrocatalysis. We have studied the symmetric and asymmetric supercapacitor cell assemblies using the high surface area porous nickel and its corresponding nickel oxide obtained by electrochemical oxidation process as the electrode materials. Activated carbon with very high surface area was used as a negative electrode in asymmetric supercapacitors. The specific capacitance values of the devices were measured using cyclic voltammetry and

charge-discharge analysis. We have measured a specific capacitance value of 473 F/g (for single electrode) for the porous nickel and 57 F/g (for single electrode) for the NiO electrodes and these values exhibit a frequency dispersion. The supercapacitor cell assemblies were shown to be stable for upto 500 charge-discharge cycles. The measured ESR value is relatively high in the case of porous nickel supercapacitors, which can be minimized by optimizing the design of the cell assembly. The relaxation time constant values ranging from 0.65ms to 160ms were determined for different supercapacitor cell assemblies using electrochemical impedance spectroscopy studies. From these studies we find that the symmetric supercapacitors exhibit a faster energy delivery capability at a higher power compared to the asymmetric cell assemblies. This indicates the potential application of these materials in short duration pulse devices.

We have also shown that the porous nickel can be used as a hydrogen-evolving cathode in electrocatalysis using Tafel plot analysis, which is the measure of current-potential characteristics of an electrode material. We have compared the measured values of the porous Ni with the other existing Ni electrocatalysts such as sintered Ni, Raney Ni and nickel material obtained using HIPE template. From the results, it can be noted that the current density per geometric area and current density per unit mass of deposited Ni for the high surface area porous nickel studied in this work is higher when compared to other materials that have been mentioned above. Also the utilization of effective electrode surface area is higher for the porous Ni with a good accessibility of electrolyte and wettability of the surface. These results demonstrate the effectiveness of this material to perform as a good electrocatalyst.

## References

1. (a) B.E. Conway, *J. Electrochem. Soc.*, 138, (1991), 1539. (b) B.E. Conway, V. Birss, J. Wojtowicz, *J. Power Sources*, 66, (1997), 1.
2. (a) I. Tanahashi, A. Yoshida, A. Nishino, *J. Electrochem. Soc.*, 137, (1990), 3052. (b) J.P. Zheng, T.R. Jow, *J. Electrochem. Soc.*, 142, (1995), L6.
3. R. Kotz, M. Carlen, *Electrochim. Acta*, 45, (2000), 2483.
4. E.E. Kalu, T.T. Nwoga, V. Srinivasan, J.W. Weidner, *J. Power Sources*, 92, (2001), 163.
5. A.F. Burke, *J. Power Sources*, 91, (2000), 17.
6. K. Rajendra Prasad, N. Munichandraiah, *Electrochem. Solid State Lett.*, 5, (2002), A271.
7. A. Rudge, J. Davey, I. Raistrick, S. Gottesfeld, *J. Power Sources*, 47, (1994), 89.
8. B.E. Conway, *Electrochemical Supercapacitors*, Kluwer Academic/ Plenum Publishers, New York, (1999), p. 1.
9. T. Morimoto, K. Hiratsuka, Y. Sanada, K. Kurihara, *J. Power Sources*, 60, (1996), 239.
10. A. Du Pasquier, J.A. Shelburne, I. Plitz, F. Badway, A.S. Gozdz, G. Amatucci, *Proceedings of the 11<sup>th</sup> International Seminar on Double Layer Capacitors and Similar Energy Storage Devices*, Deerfield Beach, FL, December, 3-5, 2001.
11. Q.L. Fang, D.A. Evans, S.L. Roberson, and J.P. Zheng, *J. Electrochem. Soc.*, 148, (2001), A833.
12. I.D. Raistrick and R.T. Sherman, in *Electrode Materials and Processes for Energy Conversion and Storage*, S. Srinivasan, S. Wagner, H. Wroblowa,

Editors, PV 87-12, *The Electrochemical Society Proceedings Series*, Pennington, NJ, (1987), pp. 582.

13. A. Laforgue, P. Simon, J.F. Fauvarque, J.F. Sarrau, and P. Lailier, *J. Electrochem. Soc.*, 148, (2001), A1130.
14. M. Mastragostino, C. Arbizzani, R. Paraventi, and A. Zanelli, *J. Electrochem. Soc.*, 147, (2000), 407.
15. A. Di Fabio, A. Giorgi, M. Mastragostino, and F. Soavi, *J. Electrochem. Soc.*, 148, (2001), A845.
16. A.J. Bard, and L.R. Faulkner, *Electrochemical Methods: Fundamentals and applications*, Wiley, New York, (1980).
17. K.C. Liu, M.A. Anderson, *J. Electrochem. Soc.*, 143, (1996), 124.
18. S.T. Mayer, R.W. Pekela, J.L. Kaschmitter, *J. Electrochem. Soc.*, 140, (1993), 446.
19. J.P. Zheng, P.J. Cygan, T.R. Zow, *J. Electrochem. Soc.*, 142, (1995), 2699.
20. V. Srinivasan, J.W. Weidner, *J. Electrochem. Soc.*, 144, (1997), L210.
21. V. Srinivasan, J.W. Weidner, *J. Electrochem. Soc.*, 147, (2000), 880.
22. K.W. Nam, K.B. Kim, *J. Electrochem. Soc.*, 149, (2002), A346.
23. C. Lin, J.A. Ritter, B.N. Popov, *J. Electrochem. Soc.*, 145, (1998), 4097.
24. S.C. Pang, M.A. Anderson, T.W. Chapman, *J. Electrochem. Soc.*, 147, (2000), 444.
25. J.H. Park, O. Ok Park, K.H. Shin, C.S. Jin, J.H. Kim, *Electrochem. Solid State Lett.*, 5, (2002), H7.
26. P.A. Nelson, J.R. Owen, *J. Electrochem. Soc.*, 150, (2003), A1313.
27. M. Bursell, A. Lundblad, P. Bjornbom, *Electrochem. Soc. Proc.*, 7, (2002), 116.
28. V. Ganesh, V. Lakshminarayanan, *Electrochim. Acta*, 49, (2004), 3561.
29. V. Ganesh, V. Lakshminarayanan, S. Pitchumani, *Electrochem. Solid State*

- Lett.*, 8 (6), (2005), A308.
30. I.J. Brown, S. Sotiropoulos, *Electrochim. Acta*, 46, (2001), 2711.
  31. K.W. Nam, W.S. Yoon, K.B. Kim, *Electrochim. Acta*, 47, (2002), 3201.
  32. K.R. Prasad, N. Miura, *Electrochem. Commun.*, 6, (2004), 849.
  33. J.H. Chen, W.Z. Li, D.Z. Wang, S.X. Yang, J.G. Wen, Z.F. Ren, *Carbon*, 40, (2002), 1193.
  34. V. Subramanian, S.C. Hall, P.H. Smith, B. Rambabu, *Solid State Ionics*, 175, (2004), 511.
  35. K.R. Prasad, N. Miura, *Electrochem. Commun.*, 6, (2004), 1004.
  36. B.E. Conway, H.A. Kozłowska, M.A. Sattar, B.V. Tilak, *J. Electrochem. Soc.*, 130, (1983), 1825.
  37. R. Juskenas, I. Valsiunas, V. Jasulaitiene, V. Pakstas, *Electrochim. Acta*, 47, (2002), 4239.
  38. L.O. Valoen, S. Sunde, R. Tunold, *J. alloys Compd.*, 253, (1997), 656.
  39. B.E. Conway, W.G. Pell, *J. Power Sources*, 105, (2002), 169.
  40. D. Qu, H. Shi, *J. Power Sources*, 74, (1998), 99.
  41. H.K. Song, Y.H. Jung, K.H. Lee, L.H. Dao, *Electrochim. Acta*, 44, (1999), 3513.
  42. H. Keiser, K.D. Beccu, M.A. Gutjahr, *Electrochim. Acta*, 12, (1976), 539.
  43. P.L. Taberna, P. Simon, J.F. Fauvarque, *J. Electrochem. Soc.*, 150, (2003), A292.
  44. E. Lust, A. Janes, M. Arulepp, *J. Electroanal. Chem.*, 562, (2004), 33.
  45. K.S. Cole, R.H. Cole, *J. Chem. Phys.*, 9, (1941), 341.
  46. J. Miller, *Proceedings of the Eighth International Seminar on Double Layer Capacitors and Similar Energy Storage Devices*, Deerfield Beach, FL, December, 7-9, (1998).
  47. S. Mitra, A.K. Shukla, S. Sampath, *Electrochem. Solid State Lett.*, 6, (2003),

A149.

48. S. Trasatti, in *Advances in Electrochemical Science and Technology*, H. Gerischer, C.W. Tobias, Editors, VCH, Verlagsgesellschaft, Weinheim, Vol. 2, (1990), p. 1.
49. J. Van Muylder, in *Comprehensive Treatise of Electrochemistry*, J.O.M. Bockris, B.E. Conway, E. Yeager, R.E. White, Editors, Plenum Press, New York, Vol. 4, (1981), p. 1.
50. E. Justi, M. Pilkuhn, W. Scheibe, A. Winsel, *Akad. Wissenschaften und Literatur*, Braunschweig, Abhandlg, Mathem. Naturwiss., Klasse, 8, (1959).
51. R. Simpraga, G. Tremiliosi-Filho, S.Y. Qian, B.E. Conway, *J. Electroanal. Chem.*, 424, (1997), 141.
52. S. Rausch, H. Wendt, *J. Electrochem. Soc.*, 143, (1996), 2852.
53. I.J. Brown, S. Sotiropoulos, *J. Appl. Electrochem.*, 30, (2000), 107.
54. S. Trasatti, in: *Advances in Electrochemical Science and Engineering*, H. Gerischer, C.W. Tobias, Editors, VCH, Weinheim, Vol. 2, (1992), p. 38.
55. S.A.S. Machado, L.A. Avaca, *Electrochim. Acta*, 39, (1994), 1385.
56. R. Simpraga, B.E. Conway, *Electrochim. Acta*, 43, (1998), 3045.
57. A.N. Correia, S.A.S. Machado, *Electrochim. Acta*, 43, (1998), 367.